A novel mitochondriotoxic small molecule that selectively inhibits tumor cell growth

Valeria R. Fantin,[1,4] Marcelo J. Berardi,[2] Luca Scorrano,[3] Stanley J. Korsmeyer,[3,4] and Philip Leder[1,4,5]

[1]Department of Genetics, Harvard Medical School, Boston, Massachusetts 02115
[2]Department of Molecular and Cellular Biology, Harvard University, Cambridge, Massachusetts 02138
[3]Department of Pathology and Medicine, Harvard Medical School, Dana Farber Cancer Institute, Boston, Massachusetts 02115
[4]Howard Hughes Medical Institute, Boston, Massachusetts 02115
[5]Correspondence: leder@rascal.med.harvard.edu

Summary

Tumorigenesis results from events that impinge on a variety of collaborating metabolic pathways. To assess their role in this process, we utilized a cell-based assay to perform a high-throughput, chemical library screen. In so doing, we identified F16, a small molecule that selectively inhibits proliferation of mammary epithelial, *neu*-overexpressing cells, as well as a variety of mouse mammary tumor and human breast cancer cell lines. F16 belongs to a group of structurally similar molecules with a delocalized positive charge. The compound is accumulated in mitochondria of responsive cells, driven by the membrane potential, and it compromises their functional integrity. Mitochondrial hyperpolarization is a shared feature of many tumor cell lines, explaining the broad action spectrum of this novel delocalized lipophilic cation.

Introduction

The *HER-2/erbB-2/neu* proto-oncogene is a member of the epidermal growth factor (EGF) receptor family. This group of receptor tyrosine kinases plays an essential role during growth and differentiation of many tissues, and its overexpression is associated with several types of human cancers (Hynes and Stern, 1994; Olayioye et al., 2000; Rubin and Yarden, 2001). Among human breast cancers, the *HER-2* gene is amplified and the protein overexpressed in 20%–30% of cases, and this event correlates with poor prognosis (Yarden, 2001). Targeted expression of constitutively active *neu*, the *HER-2* rat oncogenic allele, to the mouse mammary gland induces the appearance of multifocal mammary tumors in females harboring the transgene (Muller et al., 1988). Furthermore, *HER-2* antisense treatment in *HER-2*-overexpressing cells leads to an increase in apoptosis, demonstrating that this proto-oncogene is involved in both proliferation and survival (Roh et al., 2000). Altogether, these observations strongly suggest that HER-2/Neu plays a direct role in the development of mammary gland tumors.

The fact that repression of HER-2 tyrosine kinase suppresses the malignant phenotype of cells overexpressing the oncogene, together with its extracellular accessibility, has made this protein an excellent therapeutic target. These observations prompted the development of reagents that directly affect HER-2 activity as a means to interfere with tumor cell growth. The search for small molecules that act as ATP competitive inhibitors and natural tyrosine kinase inhibitors has yielded several compounds still under development (Noonberg and Benz, 2000; Seymour, 2001; Zwick et al., 2001). Neutralizing monoclonal antibodies directed against the extracellular domain of HER-2 have also been shown to reduce HER-2 protein level and kinase activity. Herceptin®, the humanized recombinant version of the mouse monoclonal 4D5, is currently being used for the treatment of patients with *HER-2*-overexpressing breast tumors with significant, yet limited, clinical efficacy. This antibody holds out promising results when used in combination therapies rather than as a first line-single agent therapeutic (Baselga, 2001; Winer and Burstein, 2001). Even though the mechanism of action of Herceptin® in vivo is still under investigation, extensive characterization of its effects has been carried out in cell culture. Work done using 4D5 on a panel of cell lines that express high levels of HER-2 protein demonstrated that the antibody treatment led in all cases to HER-2 dephosphorylation and downregulation, but did not always result in growth inhibition. It also demonstrated that activation of EGF-receptor family members HER-1/EGFR and HER-3/ErbB-3 and downstream signaling cascades could influence the overall response

SIGNIFICANCE

We have used mammary epithelial cells with a defined genetic alteration in a screen to isolate compounds with selective properties against an array of transformed cells. We have taken advantage of the physicochemical properties of a small molecule to establish its molecular mechanism of action. In addition, we have observed that a correlation exists between cellular transformation induced by certain oncogenes and the increase in mitochondrial transmembrane potential, which serves as the selective driving force for accumulation of the compound. Thus, this work highlights the power of cell-based assays to search for novel molecules with therapeutic potential as well as to uncover biological properties that distinguish normal from transformed cells and that could be exploited to target tumor cells selectively.

of cells to HER-2 inactivation by monoclonal antibodies (Lane et al., 2000; Neve et al., 2001). The data suggest that the activation of parallel or downstream pathways cooperating with HER-2 to induce cellular transformation may override cell growth control independently of HER-2 status. In that regard, perturbation of these essential pathways instead of or in addition to targeting HER-2 itself may provide an alternative way to inhibit propagation of *HER-2*-overexpressing cells. Furthermore, if these pathways are sufficiently conserved across different tumor types, they might also provide targets to inhibit the growth of many different cancers.

In an attempt to find novel approaches to identify those poorly understood events that collaborate with HER-2 to promote cellular transformation, we screened a chemical library using a modification of a cell-based assay involving BrdU incorporation as a measure of cell proliferation (Stockwell et al., 1999). For that purpose, we stably expressed constitutively active *neu* in EpH4 mouse mammary epithelial cells (Reichmann et al., 1992). Control EpH4 and EpH4 *neu*-overexpressing cells were screened in parallel. This strategy allowed discrimination of selective inhibitors of cell growth from general cytotoxic/cytostatic compounds. Among the small molecules isolated during our screen, F16 was the most potent growth inhibitor of the *neu*-overexpressing cells. Further characterization of this compound showed that it is selectively concentrated by mitochondria of various cell lines derived from mammary tumors of *neu* and v-Ha-*ras* transgenic mice, but not by mitochondria of normal mammary epithelial cells or various tumor cell lines derived from c-*myc* transgenic mice.

Mitochondria have been recently recognized as integrators of a plethora of intrinsic and extrinsic apoptotic pathways (Gross et al., 1999). Besides their role in apoptosis, mitochondria are essential to provide ATP for all cellular endoergonic processes. Electrons extracted from reducing equivalents generated in the matrix by the tricarboxylic acid (TCA) cycle are funneled through the mitochondrial respiratory chain complexes to finally reduce O_2. At the level of individual complexes, the transport of electrons is coupled to proton pumping into the intermembrane space. As a result of this process, a characteristic negative proton electrochemical gradient across the inner membrane is generated. The free energy accumulated in the proton gradient is used to generate ATP. The electrical portion of the gradient, the membrane potential ($\Delta\psi_m$), can vary among metabolic statuses of the cell and among different cell types, tumor carcinoma cells often being among those with higher mitochondrial membrane potential (Bernal et al., 1982; Summerhayes et al., 1982). Disruption of $\Delta\psi_m$ causes secondary perturbation of ionic and volumetric homeostasis and impedes the mitochondrial participation in crucial cellular processes such as Ca^{2+} signaling, energy production, and control of the redox state (Bernardi et al., 1999). The intrinsic variation of the $\Delta\psi_m$ among cell types and the crucial role of this parameter in mitochondrial homeostasis provide a unique opportunity for selective drug accumulation into tumor cells with potential therapeutic effect. In fact, earlier studies have shown that the constitutively higher $\Delta\psi_m$ of transformed cells could be used to selectively target toxic delocalized lipophilic cations (DLCs) that accumulate in their mitochondria in response to $\Delta\psi_m$ (Bernal et al., 1982; Nadakavukaren et al., 1985).

Our results indicate that F16 is a novel and rather different DLC characterized by very low binding to mitochondrial membranes, resulting in an almost complete accumulation in the mitochondrial matrix in response to elevated $\Delta\psi_m$. F16 displays low intrinsic toxicity, so it perturbs mitochondrial homeostasis only when its matrix levels are high (i.e., only at high $\Delta\psi_m$). The accumulation of F16 in the matrix ultimately leads to depolarization, opening of the permeability transition pore (PTP) with loss of mitochondrial structural integrity, cytochrome *c* release, cell cycle arrest, and death of the target cells. Finally, the selective effect of F16 toward *neu*-, *ras*-, and β-*catenin*-initiated mouse mammary epithelial tumor cell lines further suggests that a relationship between expression of certain oncogenes, $\Delta\psi_m$, and response to DLC might exist.

Results

A screen for small molecules with selective antiproliferative activity in *neu*-transformed cells

The transforming *neu* cDNA (*neu*^{T}) was transfected into the immortalized mammary epithelial cell line EpH4 (Figure 1A). By Western blot analysis, an increase in the phosphorylated form of MAP kinase and PKB was observed in the *neu*-overexpressing cells using antibodies that specifically recognize the phosphorylated active form of the proteins (Figure 1B). Expression of *neu*^{T} altered the morphology of EpH4 cells in two-dimensional cultures (Figure 1C). In addition, *neu*-overexpressing cells, but not EpH4 alone, formed fast-growing tumors when injected into nude mice (data not shown). These results indicated that Neu protein was capable of active signaling and of inducing cellular transformation in the EpH4 cells. These stably transfected cells provided a good experimental system to utilize in a high-throughput screen (HTS) for inhibitors that selectively interfere with the proliferation of *neu*-overexpressing cells. A chemical library comprised of approximately 16,000 small molecules was screened using the cytoblot assay. The ability of small molecules to inhibit cell proliferation at a final concentration of 10–15 μM was determined by the relative incorporation of BrdU into DNA in EpH4-A6 (A6) *neu*-overexpressing and EpH4-EV (EV) control cells. The results for one particular set of 4 plates from the 51 sets tested during the screen are shown (Figure 1D). In this specific example, several small molecules exhibited an antiproliferative effect on *neu*-expressing cells which was indistinguishable from that exhibited on control cells. In only one instance, a small molecule affected proliferation of the transformed cells in a selective manner. Several compounds, which scored as positives during the initial screen, could be clustered into groups based on structural homologies. During a secondary screen, the potency of these small molecules was evaluated at 1 μM. Out of the six compounds selected, one that we termed F16 was capable of partially inhibiting BrdU incorporation in EpH4-A6 at a concentration of 100 nM in a dose-response assay (Figure 1E).

F16 affects growth in several mouse and human cancer cell lines

The effect of F16 on a panel of mouse tumor cell lines derived from *neu*, v-Ha-*ras*, β-*catenin*, and c-*myc* transgenics and a panel of breast human cancer cell lines was assessed. Cell lines were scored as positives if they showed a 2–5 fold reduction in the total cell number after 3 days and 10–40 fold reduction after 7 days. Among the mouse cell lines tested, those derived from mammary tumors from *neu* and *ras* transgenic mice exhib-

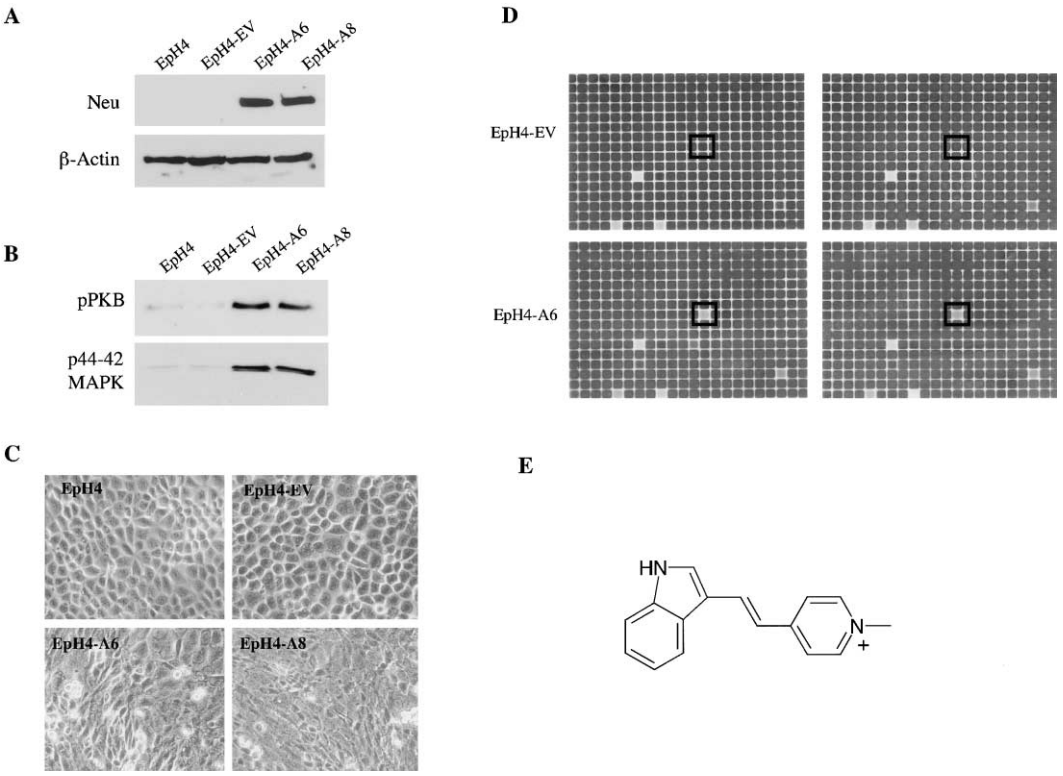

Figure 1. Characterization of EpH4 cells stably expressing *neu* and cytoblot screen

A: Whole cell lysates from starved parental EpH4, two *neu*-overexpressing clones (EpH4-A6 and EpH4-A8), and control cells transfected with the empty vector (EpH-4-EV) were prepared as described in the Experimental Procedures. Equivalent amounts of proteins were resolved by SDS-PAGE and immunoblotted with antibodies against Neu and β-actin. **B:** Samples were further immunoblotted with antibodies against the phosphorylated forms of PKB and MAPK. **C:** Phase contrast image of clones in 2D cultures. **D:** EpH4-EV (top) and EpH4-A6 *neu*-overexpressing cells (bottom) were screened in parallel using a chemiluminescent-based assay (Experimental Procedures) for the ability of small molecules to inhibit BrdU incorporation as a measure of their growth inhibitory effect. The autoradiograph shows one example of a set of plates from the 51 sets screened. The well highlighted in black corresponds to a small molecule with selective antiproliferative effect on the *neu*-transformed cells. **E:** Structure of F16, the most potent inhibitor isolated during HTS.

ited a marked sensitivity for F16, while the growth of the mouse fibrosarcoma cell lines derived from *ras*-transgenic mice was not affected (Table 1). In addition, we observed a moderate response in the case of β-*catenin*-initiated mammary tumor cell lines, while *myc*-initiated mouse tumor cells were F16 resistant. Eight out of the ten cell lines in the human breast cancer panel were also affected by the small molecule (Table 1). These results demonstrated that this compound displayed antiproliferative activity against both mouse and human breast cancer cells. A positive correlation between the initiating oncogene in mouse mammary epithelial tumor cells and the response to F16 was observed. However, the resistance of fibrosarcoma tumor cells in the case of the *ras*-initiated cell lines suggests that F16 sensitivity can not be simply defined on the basis of oncogene overexpression, but rather that other factors imposed by the cellular environment play a major role in the outcome of the treatment.

Cell cycle arrest and increased apoptosis in F16-treated cells

Based on our results from the cell panel treatment and the decrease in BrdU incorporation caused by F16 in *neu*-overexpressing cells by cytoblot, we examined the effect of F16 on the cell cycle. F16 caused a dramatic decrease in the number of cells in S phase and an increase in the percentage of cells in G1 phase, as measured by FACS analysis of cells stained for DNA content with an antibody specific for BrdU (Figure 2A). These results indicated that the decrease in the BrdU incorporation observed during the HTS is consistent with a cell cycle arrest. Cell cycle analysis performed on mouse and human cell lines that scored sensitive to F16 in the viability assay showed a similar dramatic decrease in the number of cells in S phase with a consistent G1 arrest for most cases, and both G1 and G2 in a few instances (data not shown). So in addition to the effects observed in A6 and A8 EpH4 *neu*-overexpressing cells, F16 induced cell cycle arrest in sensitive mouse tumor and human cancer cell lines. Prolonged incubation with 3 μM F16 resulted in increased cell death of F16-sensitive cells but not of F16-resistant ones. Hence, we assessed if cell death by apoptosis followed the cell cycle arrest observed upon F16 treatment. While the EV cells were not affected, F16 caused apoptosis of A6 cells in a time-dependent manner, as judged by oligonucleosomal DNA fragmentation (Figure 2B). The Annexin V staining assay showed that after a 24 hr treatment with F16, A6 cells were still viable, and that a subpopulation was already undergoing apoptosis (Annexin V-PE positive, 7-AAD negative) (Figure 2C). Longer incubation of A6 cells in the presence of the small molecule resulted in an increase in the Annexin V-PE and 7-AAD positive cell population, indicative of cells in later

Table 1. Effect of F16 on mouse and human tumor cell lines

Organism	Initiating oncogene	Cell line	Tissue of origin/ tumor type	F16 response
Mouse	*neu*	NF980	Breast	+
		SMF	Breast	+
		NAF	Breast	+
		n-Neu	Breast	+
		Neu4145	Breast	+
		NF324-2A	Breast	+
		NF324-1B	Breast	+
	v-Ha-*ras*	AC/Balb12	Fibrosarcoma	−
		AC/Balb14	Fibrosarcoma	−
		AC/Balb6.6	Fibrosarcoma	−
		AC/p53$^-$ #16	Fibrosarcoma	−
		AC/p53$^-$ #19	Fibrosarcoma	−
		AC260	Jaw	−
		AC99	Neck	−
		AC222	Intestinal	−
		AC/p53$^-$ 4782	Intestinal	−
		AC/p53$^-$ #1	Salivary	−
		AC816	Breast	+
		AC711	Breast	+
		AC236	Breast	+
		SH1.1	Breast	+
	β-*catenin*	9281.a	Breast	+/−
		5297.B1	Breast	+/−
		5281.1	Breast	+/−
		5297.A2	Breast	+/−
	c-*myc*	16MB9a	Breast	−
		Myc 83	Breast	−
		M158	Breast	−
		13MA1a	Breast	−
Human	Unknown	SKBR-3	Breast	+
		T47D	Breast	+
		ZR75	Breast	+
		BT474	Breast	+
		MCF-7	Breast	+
		MDA-MB-231	Breast	−
		MDA-MB-435	Breast	−
		MDA-MB-436	Breast	+
		MDA-MB-453	Breast	+
		MDA-MB-468	Breast	+

+, >10 fold difference in cell number.
+/−, 2- to 4-fold difference in cell number.
−, no difference in cell number.

stages of apoptosis or cells that had already died. In contrast, untreated or F16-treated control cells were primarily viable and not undergoing apoptosis (AnnexinV-PE, 7-ADD negative). Many intrinsic apoptotic stimuli converge on the mitochondria and induce the release of cytochrome *c* to activate downstream pathways of the cell death program (Liu et al., 1996). We therefore measured whether F16 induced the release of cytochrome *c* from the mitochondria by specific immunofluorescence. Of note, F16 induced early cytochrome *c* release, with loss of the punctate mitochondrial pattern for cytochrome *c* and the appearance of a diffuse cytosolic staining (Figure 2D). In conclusion, following cell cycle arrest, F16 treatment led to apoptotic death of F16-sensitive EpH4-A6 cells, but not of F16-resistant EpH4-EV cells.

F16 is a fluorescent small molecule that can be visualized in living cells

Pyridinium ions and indole produce absorption and emission bands in the UV region of the electromagnetic spectrum, but due to the extended π electron system created by the link of the two rings, F16 shows a lower energy absorption band in the visible region with a maximum at 420 nm. Relaxation of the exited state by fluorescence is also favored by the conformational rigidity of the molecule, resulting in an intense emission band at 520 nm. These properties allowed the direct visualization of F16. We have used its autofluorescence to determine the fate of the molecule inside the cell. Various cell lines incubated with F16 for 24 hr were examined for their fluorescent signal under an inverted microscope. Immortalized, nontransformed mouse mammary epithelial cell lines like HC11, NMuMG, and EpH4, human mammary epithelial MCF10A, and mouse tumor cell lines initiated by the c-*myc* oncogene, which are unaffected by F16, did not show any uptake/retention of the compound. In contrast, the F16-sensitive EpH4 *neu*-overexpressing clones A6 and A8, and the v-Ha-*ras*-, *neu*-, and β-*catenin*-initiated tumor cell lines, showed an intracellular green fluorescent punctated staining pattern suggestive of F16 targeting to intracellular structures or organelles (Figures 3A–3B). When cells were costained with specific mitochondrial and lysosomal probes, the F16 fluorescence perfectly overlapped with the mitochondrial staining, but not with the lysosomal one (Figures 4A–4B). Besides the mitochondria, some dense nuclear particles, potentially the nucleoli, were also weakly stained as previously reported for other lipophilic fluorescent cations such as Rhod2 and Mitotracker Orange (Boitier et al., 1999; Scorrano et al., 1999). These results indicated that the mitochondria were the major F16-concentrating organelle in the cell. Taken together with the ability of F16 to induce cytochrome *c* release, these results pointed to mitochondria as a potential site of action for F16.

Selective accumulation of F16 in mitochondria is driven by their negative transmembrane potential

As mentioned earlier, a group of molecules collectively known as delocalized lipophilic cations or DLCs that, like F16, selectively accumulate in the mitochondria of tumor cells had been previously described (Modica-Napolitano and Aprille, 2001). Rhodamine 123, the thiopyrylium AA-1, and the rhodacyanine MKT-077 all share a highly hydrophobic structure and a delocalized positive charge that allows for their diffusion through lipid membranes and their accumulation. While chemically very different in overall structure from these compounds, in this particular regard, F16 resembles these DLCs.

We therefore tested whether the $\Delta\psi_m$ was the driving force for F16 accumulation into the mitochondria. Preincubation of A6 cells in medium containing carbonyl cyanide p-(trifluoromethoxy)phenylhydrazone (FCCP), a protonophore that dissipates the $\Delta\psi_m$, or valinomycin, a K^+-ionophore, retarded the entry and greatly reduced the overall accumulation of F16 inside mitochondria. Furthermore, if FCCP was added to cells preloaded with F16, F16 mitochondrial staining was immediately lost and a diffuse signal throughout the cytoplasm emerged instead. This suggests that the $\Delta\psi_m$ is not only promoting F16 entrance but it is also acting as a retention force to drive the accumulation (Figure 5A). In addition, preincubation of cells in the presence of high K^+ medium (150 mM) to depolarize the plasma membrane resulted in a delayed F16 appearance inside mitochondria (data not shown). These results further suggests that the plasma membrane, as previously observed with other DLCs, might help to preconcentrate F16 in the cytoplasm of

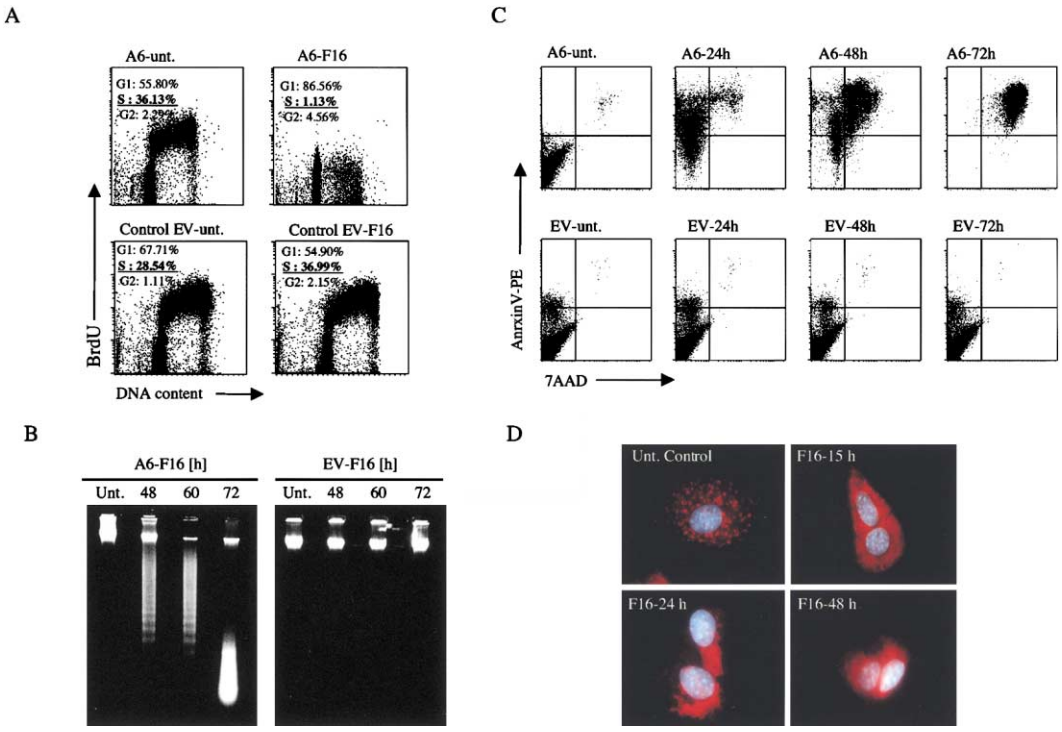

Figure 2. Cell cycle analysis and determination of apoptosis on F16-treated cells

A: Flow cytometry analysis of BrdU incorporation in EpH4-A6 and control EV cells treated with 3 μM F16 for 36 hr. **B:** Agarose gel electrophoresis followed by ethidium bromide staining of DNA isolated from untreated or EpH4-A6 cells treated with F16 for 48, 60, and 72 hr. **C:** EpH4-A6 and control EV cells subjected to a time-course treatment with F16 were stained with Annexin V-PE in buffer containing 7-AAD and analyzed by FACS. **D:** Subcellular localization of cytochrome *c* by immunofluorescence in untreated or F16-treated EpH4-A6 cells for 15, 24, and 48 hr.

sensitive cells, which in turn moves into the mitochondrial matrix that is at a more negative potential. Most of the currently used fluorescent $\Delta\psi_m$ probes are substrates for the plasma membrane multidrug resistance pumps that can efficiently extrude them from the cytosol. To determine if the lack of F16 accumulation inside the F16-insensitive cells was due to active extrusion by the multidrug resistance pumps, F16-resistant immortal mammary epithelial and human breast cancer cell lines were coincubated with 3 μM F16 in the presence of 10 μM verapamil/100 μM probenecid. Under these conditions, F16 did not accumulate in mitochondria, indicating that at least in the cell lines examined, the exclusion was not mediated by MDR-1 or MRP-1 (Lizard et al., 1994).

Because cellular accumulation of F16 appeared to be a function of the $\Delta\psi_m$, and it was not influenced by multidrug resistance pumps, we compared in a semiquantitative way the mitochondrial potential among cell lines that are sensitive or resistant to F16. For this purpose, A6 cells, control cells, and various mouse tumor cell lines were subjected to flow cytometric analysis using tetramethylrhodamine methyl ester (TMRM), a probe whose accumulation in the mitochondrial matrix is proportional to the $\Delta\psi_m$. Nonyl-acridine orange, a probe that stains the mitochondrial lipid cardiolipin, was used to normalize according to mitochondria mass (Table 2). The results from these experiments showed that cell lines that responded to F16 accumulated 2.5–25 fold more TMRM than insensitive ones. In situ mitochondrial TMRM fluorescence in *neu*-overexpressing cells appeared clearly higher than in the control EV cells, further confirming the flow cytometry analysis (Figure 5B). The protonophore FCCP completely abolished the punctate mitochondrial pattern of TMRM to an equivalent level in A6 and EV cells, indicating no significant differences in the binding of the probe between the two cell lines (data not shown). In light of the previous results, we concluded that there was a direct correlation between intensity of TMRM staining, i.e., resting mitochondrial membrane potential, F16 accumulation, and the sensitivity of cells toward it.

Mitochondrial structure and function are compromised in cells affected by F16

To test whether F16 concentration compromised mitochondrial homeostasis, we performed electron microscopy analysis on untreated or F16-treated A6 cells, control cells, and two additional mouse tumor cell lines, SH1.1 and SMF. Mitochondria were the only organelles where ultrastructural abnormalities were evident as early as 15 hr of F16 treatment. A6 cells showed progressive swelling, disruption of the mitochondrial cristae, and concomitant mitochondrial outer membrane rupture, while EV cells showed no lesions (Figure 6A). One of the major roles of mitochondria is to supply energy to the cell. To assess alterations in mitochondrial function, ATP levels were determined in F16-treated cells by the luciferase-catalyzed ATP-dependent bioluminescent oxidation of luciferin (Figure 6B). A significant depletion in the ATP pool was observed in cells after 24 hr of F16 incubation. Mitochondria are the major intracellular source of reactive oxygen species, which are expected to be more

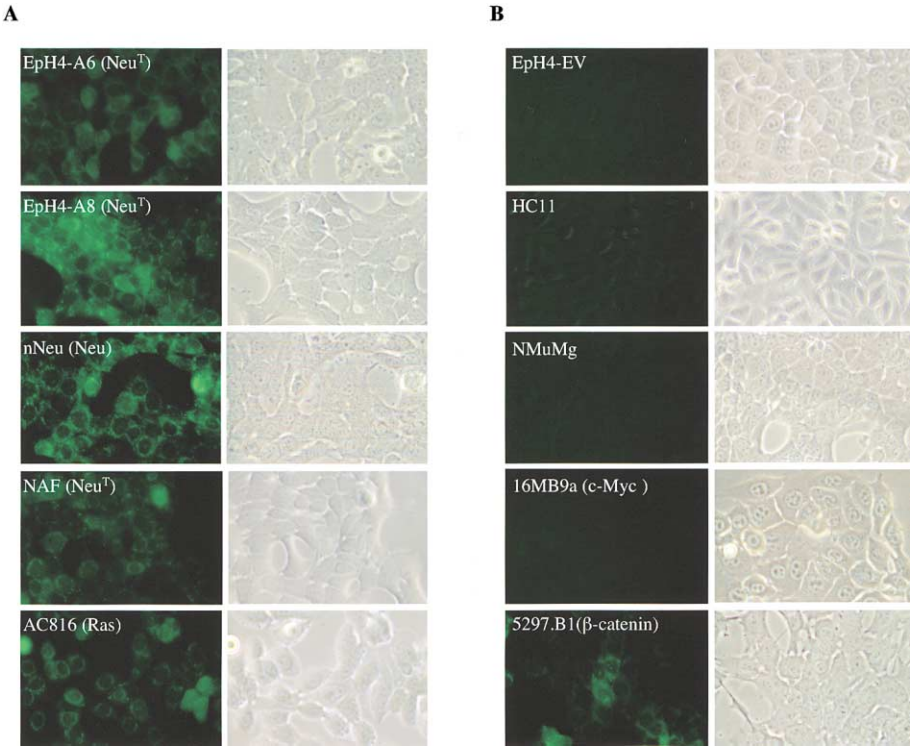

Figure 3. Imaging F16 in living cells

A: A panel of F16-sensitive mouse mammary tumor cell lines was incubated in 3 μM F16-containing medium for 24 hr prior to imaging. **B:** F16 fully resistant immortalized mouse mammary epithelial and partially resistant tumor cell lines subjected to identical treatment. Fluorescent F16 signal on the left; phase contrast on the right.

abundant during apoptosis and in response to mitochondrial dysfunction (Raha and Robinson, 2001). We therefore measured the level of superoxide anion following treatment with F16. An increase in superoxide production could be detected by monitoring the conversion of dihydroethidium to ethidium by flow cytometry (Figure 6C). The increase in the fluorescent signal observed in F16-treated A6 cells but not in EV cells as a consequence of the resulting complex between ethidium-DNA is indicative of higher levels of superoxide anion. These results are in accordance with the observed F16-dependent increase in cellular protein carbonyl content, an indicator of protein oxidative damage (data not shown). Since the accumulation of F16 in mitochondria is dependent on $\Delta\psi_m$, we tested whether dissipation of the membrane potential was able to interfere with F16 cytotoxicity. While A6 cell number dramatically decreased upon F16 incubation, its proliferation rate in the presence of FCCP/F16 was indistinguishable from that of FCCP alone (data not shown). Our data suggested that mitochondria were likely the primary target for F16-mediated toxicity. F16 accumulation in mitochondria induced mitochondrial damage characterized by failure to synthesize ATP, imbalance of volumetric homeostasis, cytochrome *c* release and increased production of reactive oxygen species. Thus, the volumetric, energetic, and redox balance in the F16-treated cells was drastically disrupted.

Mitochondria are a direct target for F16-mediated toxicity

Electron microscopy images showed that F16 induced mitochondrial swelling in *neu*-overexpressing cells. Therefore, we dissected the mechanism of F16-induced swelling to understand its mode of action at the molecular level. The permeability transition pore (PTP) is a nonselective, voltage-dependent inner mitochondrial membrane channel that in its open conformation is permeable to solutes up to 1500 Da (Bernardi et al., 1999). Opening of the PTP ultimately leads to swelling of mitochondria and has been suggested to be involved in several apoptotic pathways (Bernardi et al., 1999; Kroemer et al., 1998). To address if F16 affected the PTP, we turned to mouse liver mitochondria. Under the experimental in vitro conditions, in the absence of ADP, mitochondria will not use part of the proton electrochemical gradient to drive ATP synthesis. This results in a constitutively high membrane potential that can drive F16 accumulation into mitochondria. F16 caused swelling of purified mitochondria in a dose-dependent fashion, and cyclosporin A (CsA), a specific PTP inhibitor, completely abolished this effect (Figures 7A–7B) (Broekemeier et al., 1989). It has previously been shown that DLCs such as Mitotracker Orange can cause mitochondrial depolarization followed by induction of the PTP (Scorrano et al., 1999). We asked whether F16-mediated PTP opening could be the result of F16-induced mitochondrial depolarization. To address this question, we took advantage once again of the fluorescent properties of F16. Isolated mitochondria build up a membrane potential in response to energization by addition of respiratory substrates. We monitored the changes in fluorescence of a 1 μM solution of F16 in response to mitochondrial energization and depolarization. In response to mitochondrial energization, the fluorescence of the F16 solution increased, whereas membrane potential dissipation by FCCP completely reverted this fluorescence increase (Figure 7C, black trace). Interestingly, when mitochondria were incubated with 30 μM F16, energization led to a much smaller fluorescence increase (Figure 7C, green trace). Preincubation of mitochondria with the PTP inhibitor CsA only partially blunted this effect (Figure 7C, red trace). Thus, F16 caused depolarization of purified

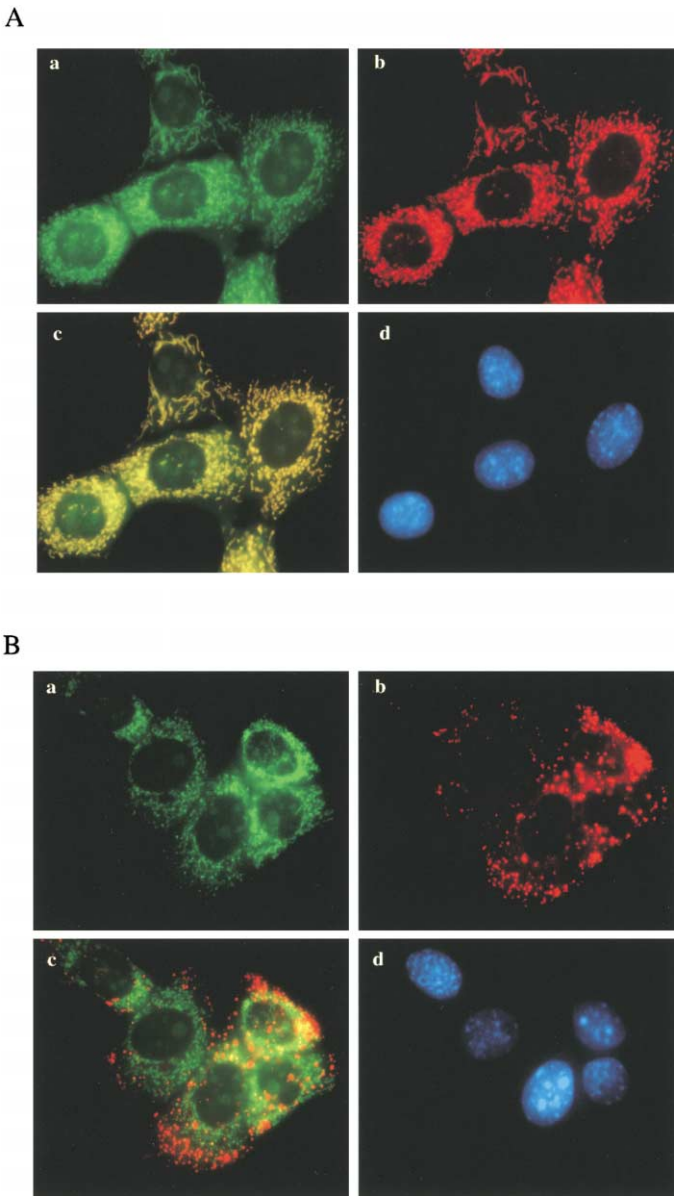

Figure 4. Colocalization of F16 and mitochondrial specific probe

A: EpH4-A6 cells were coincubated as described under "Experimental Procedures" with F16 (**a**) and Mitotracker Red (**b**) and the images overlaid (**c**). Nuclei were stained with Hoechst (**d**). **B:** Same as **A**, but with Lysotracker Red instead of Mitotracker Red.

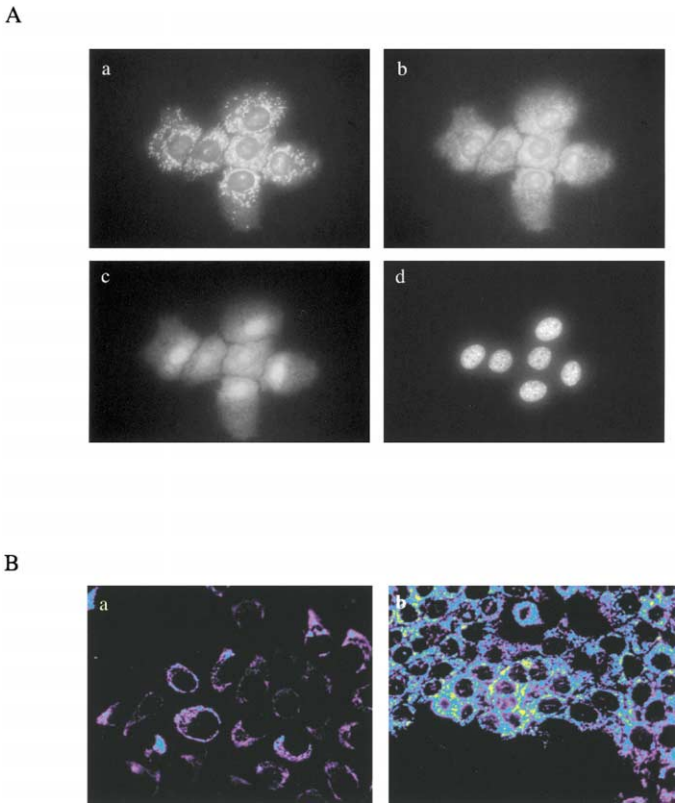

Figure 5. Effect of mitochondrial transmembrane potential ($\Delta\Psi m$) on F16 mitochondrial concentration

A: Cells were preincubated in F16-containing medium for 1 hr (**a**) and then treated with 5 μM FCCP. Cells were photographed 1 min (**b**) and 3 min (**c**) after FCCP addition. Nuclei were counterstained with Hoechst (**d**). **B:** Pseudocolor-coded images of TMRM fluorescence in control EV cells (**a**) and A6 cells (**b**). Cells were stained with TMRM and imaged as described in the Experimental Procedures.

mitochondria. This depolarization led to opening of the PTP, further increasing the dissipation of $\Delta\psi_m$. Next, we investigated the mechanism of the observed depolarization. In principle, mitochondrial depolarization could be caused by a direct protonophoric effect, i.e., by protons shuttling across the inner mitochondrial membrane, or indirectly as a consequence of inhibition of the respiratory chain. To dissect this, we assessed the effect of F16 on mitochondrial respiration by measuring mitochondrial O_2 consumption. In vitro, mitochondria respond to membrane depolarization by increasing their basal (state 4) respiratory rate. F16 caused an increase in state 4 respiration in mitochondria incubated with substrates for complexes I and II+III (Figure 7D). At higher concentrations, this increase in mitochondria energized with complex I substrates dropped in a CsA-sensitive fashion. This is due to loss of pyridine nucleotides from the mitochondrial matrix as a consequence of PTP opening rather than a direct effect of F16 on electron transfer, since no decrease in respiration was observed when mitochondria were energized with succinate (which feeds electrons directly to complex II, bypassing the need for pyridine nucleotides) (Figure 7D). Thus, our results indicate that F16 affects mitochondrial respiration, inducing an increase rather than a decrease in basal respiratory rate that would be expected following inhibition of the respiratory chain. Small perturbations on the electron transfer chain do appear manifest when measuring the basal respiratory rate, and they may become evident when electron transfer along the respiratory chain is maximized, i.e., when mitochondria are uncoupled. For this purpose, we determined the effect of F16 on uncoupled respiration. The uncoupler FCCP was added to mitochondria 3 min after F16, and the rate of uncoupled respiration was measured. Increasing concentrations of F16 caused a progressive inhibition of the uncoupled respiration, irrespective of the respiratory substrate used. The PTP inhibitor CsA completely abolished this effect (Figure 7E). Thus, the respiratory inhibition does not appear to be due to a direct effect of

Table 2. Comparison of ΔΨm in F16-sensitive and resistant cells by flow cytometry analysis of TMRM staining

Cell line	Mitochondrial potential log TMRM emission (a.u.)	Mitochondrial mass NAO ratio 530 nm/630 nm	TMRM/NAO ratio
Immortal			
EpHr	37	3.10	11.94
EpH4-EV	199	2.76	72.10
HC11	118	2.77	42.60
NMuMG	33	3.17	10.41
c-myc			
13MA1a	269	2.94	91.50
16MB9a	240	2.80	85.71
neu			
EpH4-A6	462	1.78	259.55
EpH4-A8	466	1.72	270.93
SMF	875	2.89	302.77
NAF	761	2.58	294.96
v-Ha-*ras*			
AC816	726	3.36	216.07
SH1.1	648	3.45	187.83

F16 on electron transfer, but rather the consequence of F16-induced PTP opening, which includes secondary swelling and release of the respiratory chain component cytochrome *c*. Taken together, these results show that F16 acts as a weak protonophore and that it lowers $\Delta\psi_m$. This depolarization results in opening of the voltage-dependent PTP. Opening of the PTP is followed by ionic imbalance, swelling, cytochrome *c* release, and inhibition of mitochondrial respiration, consistent with the phenotypes observed in vivo.

Since F16 causes PTP opening in isolated mitochondria, we asked whether the PTP inhibitor CsA prevented F16-induced mitochondrial toxicity in A6 cells. CsA blocked mitochondrial swelling and cytochrome *c* release induced by F16. As expected, since the inhibitory effect of CsA on the PTP is transient, the protection became increasingly weaker upon prolonged F16 incubation (data not shown). Taken together, these results suggest that the mitochondrial dysfunction induced by F16 is related to induction of the PTP.

Neu-dependent signaling is turned off in F16 treated cells

In parallel to the characterization of the effect of F16 on mitochondria homeostasis, we investigated the effect of F16 on cell signaling. A decrease in phosphotyrosine content of Neu, phosphorylated PKB/Akt, and phosphorylated MAP kinase were observed. As a consequence of F16 treatment, Neu and PKB protein levels were reduced (Figure 8). Previous studies have shown that Neu and PKB/Akt are substrates for caspase-mediated cleavage (Bachelder et al., 2001; Tikhomirov and Carpenter, 2001). Therefore, we tested whether this downregulation was blocked by the broad-spectrum caspase inhibitor zVAD-fmk. zVAD-fmk only partially inhibited Neu and PKB/Akt downregulation (data not shown). Given the profound mitochondrial dysfunction that accompanies F16-induced cytochrome *c* release, the only partial zVAD-fmk protective effect could be the result of an increase in degradation of proteins that have undergone oxidative damage. A limited cellular ATP supply leads to

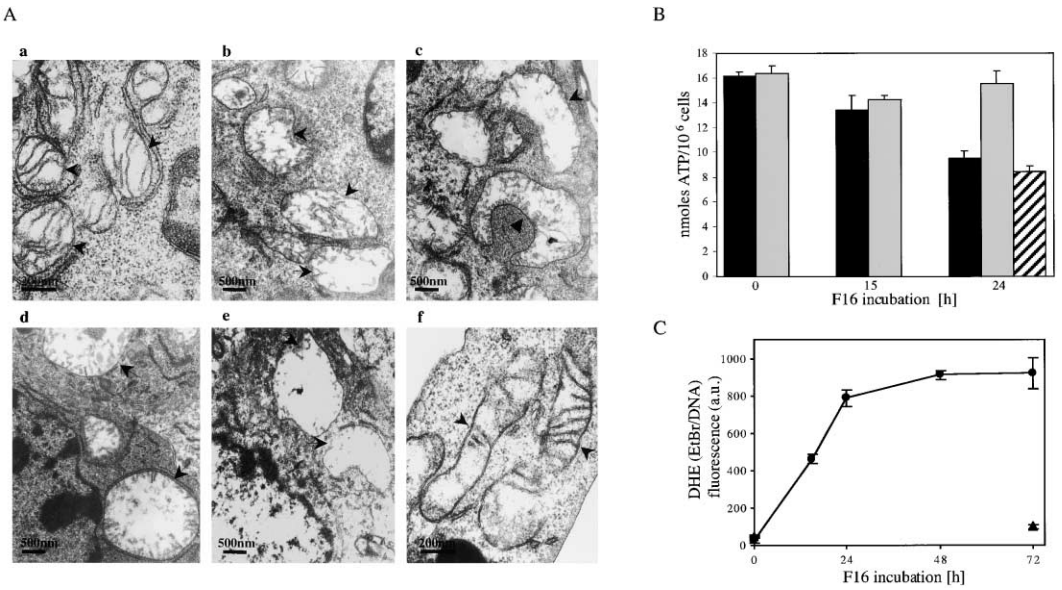

Figure 6. Structural-functional alterations in mitochondria of F16-treated A6 cells

A: Electron microscopy was performed on ultrathin sections of A6 untreated (**a**) or treated with F16 for 15, 24, 36, and 48 hr (**b**–**e**). Control EV cells were treated with F16 for 48 hr (**f**). Normal and abnormally swollen and apoptotic mitochondria in the case of F16-treated A6 cells are marked with black arrows. **B:** Quantification of ATP levels by luciferin-luciferase assay in F16-treated EpH4-A6 cells (black) and EV cells (gray) as described under Experimental Procedures. Control FCCP-treated A6 cells (hatched). **C:** Comparison of reactive oxygen intermediate levels in F16-treated EpH4-A6 (circles) and EpH4-EV (triangles) cells. Flow cytometry analysis of ethidium bromide-DNA fluorescence resulting from dihydroethidium oxidation as a measure of superoxide levels.

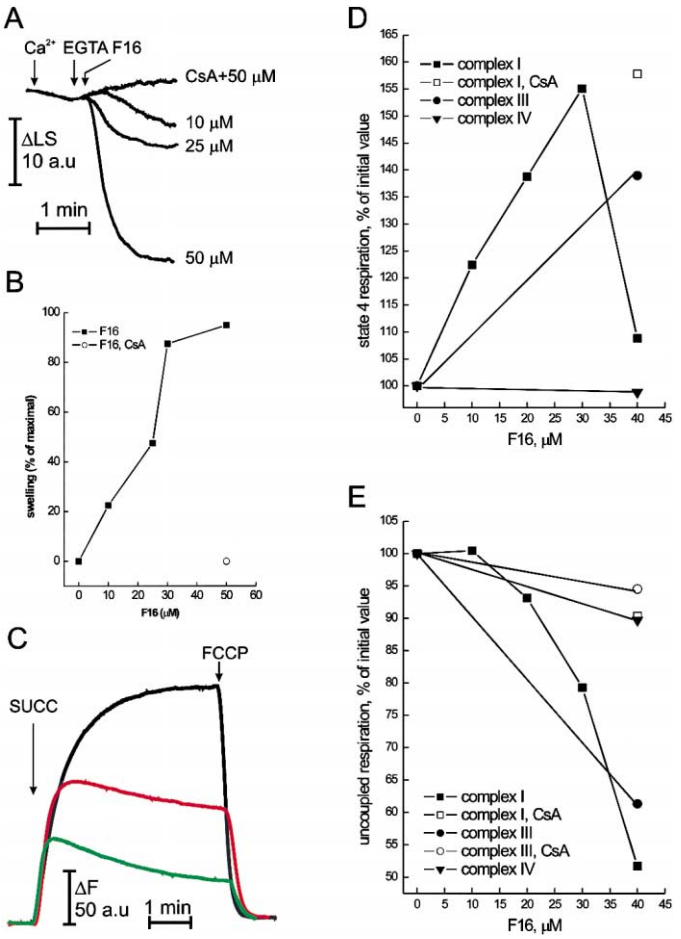

Figure 7. Effect of F16 on isolated mitochondria

A: Effect of F16 on mitochondrial volume. 0.5 mg/ml mitochondria were incubated in experimental buffer. Where indicated, 10 μM Ca^{2+}, 0.5 mM EGTA (a Ca^{2+} chelator used to synchronize PTP opening in population of isolated mitochondria) opening, and F16 were added. If indicated, 1 μM CsA was added prior to mitochondria suspension. **B:** Dose dependence of permeability transition pore induction by F16. The experiment was conducted as in **A**. **C:** Effect of mitochondrial energization on F16 fluorescence. 0.5 mg/ml mitochondria were incubated in experimental buffer supplemented with 2 μM rotenone and 1 μM (black trace) or 30 μM (red and green traces) F16. Green trace, 2 μM CsA was present from the beginning. Where indicated, 5 mM succinate and 200 nM FCCP were added. Note that mitochondrial energization causes an increase in the fluorescence of F16. **D:** Effect of F16 on basal (state 4) respiratory rate. Mitochondria (1 mg/ml) were incubated in experimental buffer supplemented with substrates for the individual respiratory complexes. Oxygen consumption was determined as described in the methods section. Where indicated, mitochondria were incubated with 1 μM CsA for 2 min before F16 addition. Respiratory rates are normalized to the rate of untreated mitochondria. Maximum rate of oxygen consumption (state 4): complex I (glutamate/malate), 10.3 ± 1.1 nAt/mg/min; complex II+III (succinate), 19.6 ± 2.1 nAt/mg/min; complex IV (ascorbate/TMPD), 110.4 ± 6.7 nAt/mg/min. **E:** Effect of F16 on uncoupled respiratory rate.1 mg/ml mitochondria were treated with 200 nM FCCP and 3 min later with the indicated concentration of F16. Respiratory rates are plotted as the percentage of the maximum rate (in the presence of FCCP alone). Maximum rate of oxygen consumption (uncoupled): complex I, 61.8 ± 4.3 nAt/mg/min; complex II+III, 127.4 ± 5.3 nAt/mg/min; complex IV, 132.5 ± 5.1 nAt/mg/min.

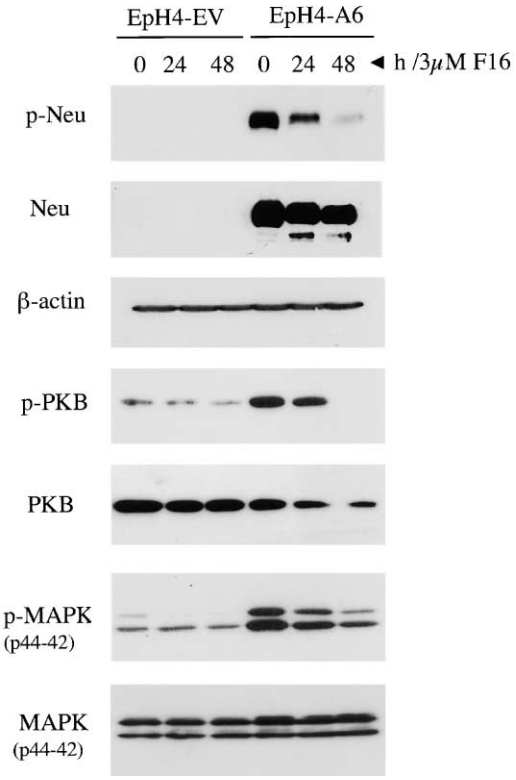

Figure 8. Effect of F16 on Neu activation and downstream signaling

Control and *neu*-overexpressing EpH4-A6 cells were left untreated or treated with 3 μM F16 for 24 and 48 hr. Whole cell lysates were prepared as described (Experimental Procedures). Samples were immunoblotted with antibodies against Neu, PKB, and MAPK, as well as antibodies that react with the phosphorylated forms of the proteins. Samples were probed with anti-β-actin as loading control.

decrease in overall protein synthesis, an ATP-dependent process. These two effects combined may affect the steady-state level of proteins in a differential manner, depending on their particular turnover rates, since MAPK and β-actin levels were not affected. Regardless of the mechanism behind F16-mediated protein downregulation and dephosphorylation, the net effect is inactivation of major pathways involved in proliferation and survival, further contributing to the inhibition of cell growth.

Discussion

The goal of the chemical screen performed was to use an unbiased assay and to identify novel small molecules that could selectively inhibit the growth of *neu*-overexpressing cells, in order to gain insights into the process of cellular transformation driven by this oncogene. These studies led to the isolation of F16, a small molecule that selectively targets *neu*-overexpressing mammary epithelial cells. Further characterization of the compound showed a broader spectrum of action. In addition to mouse mammary tumor cell lines overexpressing *neu,* mouse mammary tumor cell lines overexpressing v-Ha-*ras* and β-*catenin*, but not c-*myc*, and human breast tumor cell lines of a diverse nature were growth inhibited as well. Unlike our mouse mammary tumor cells lines, the initiating event in the human breast cancer cell lines analyzed is undefined, which makes

correlations of F16 sensitivity harder to establish. Although SKBR-3, BT474, and MDA-MB-453 express *HER-2* at high levels, the growth inhibitory effect of F16 was not limited to them. For example, cell lines like MCF-7, T47D, or MDA-MB-468, with moderate to undetectable levels of HER-2 compared to immortal mammary epithelial cells, were F16 sensitive as well. These same cell lines have been shown to overexpress various combinations of EGF receptor family members, which could explain, in part, their sensitivity toward F16 (Moasser et al., 2001). Our interpretation of the results in mouse and human cell lines is that transformation mediated by *neu*, as well as other oncogenes like v-Ha-*ras,* β-*catenin,* and potentially EGF family members, among others, could induce the changes that render cells responsive to F16.

Based on the fluorescent properties of F16, we were able to identify the mitochondria as the major concentrating organelle in the cell. This observation and the fact that F16 is a lipophilic small molecule with delocalized positive charge suggested that it is a member of the DLC group of small molecules. This group of mitochondriotoxic compounds has been defined empirically. The structural diversity among DLCs is striking and, to date, the properties that make each DLC a good antiproliferative agent are still poorly understood. At high concentration, these molecules display mitochondrial toxicity, although their targets are quite different. For instance, the toxic effects of rhodamine 123 and dequalinium chloride have been linked to their ability to inhibit F0-F1 ATPase and NADH-ubiquinone reductase activity, respectively (Anderson et al., 1989, 1993; Modica-Napolitano and Aprille, 1987; Modica-Napolitano et al., 1984). Likewise, MKT-077 toxicity has been associated with both MKT-077-driven mitochondrial DNA depletion and a general destabilization of the mitochondrial inner membrane (Modica-Napolitano et al., 1996).

Given their higher $\Delta\psi_m$, mitochondria of tumor cells specifically accumulate DLCs. Normal cells, on the other hand, possess moderate $\Delta\psi_m$ and fail to accumulate this class of compounds. F16 causes mitochondrial dysfunction as judged from our studies in cells or with purified mitochondria. Our results indicate that F16 is capable of slowly dissipating the proton gradient established across the inner mitochondrial membrane. The decrease in the $\Delta\psi_m$ can in turn be sensed by the PTP, a voltage-dependent inner membrane channel (Scorrano et al., 1997). Opening of the PTP leads to an increase permeability to small solutes and dissipation of ionic gradients, swelling, inhibition of respiration, disruption of redox homeostasis, and release of apoptogenic factors, committing the cell to apoptotic death. We assessed whether F16 retained its ability to induce apoptosis in cells lacking *bax/bak* (DKO) that are resistant to a panoply of apoptotic inducers (Wei et al., 2001). F16 was accumulated to similar levels in both cell lines, and induction of apoptosis was comparable in the two genotypes (data not shown). Our results from studies in isolated mitochondria and cells suggest that F16 toxicity is mediated, at least in part, by the PTP. Nevertheless, our studies do not exclude the possibility that in cells the prolonged, high local concentration of F16 within the mitochondrial matrix could affect the organelle at multiple levels. Thus, it is possible that F16, besides causing PTP opening, could be producing several parallel mitochondrial lesions that collectively induce cell death.

In addition to the effect of F16 on tumor cell lines in culture, we also tested the effect of F16 in vivo. Several studies have established the anticarcinoma activity of systemically administered DLCs against various tumor cell lines implanted in nude mice (Chiba et al., 1998; Koya et al., 1996; Sun et al., 1994). The potential of MKT-077 as a new antineoplastic compound was recently evaluated. Although the phase I trials were discontinued due to renal toxicity, both studies established that MKT-077 was preferentially accumulated in tumor cell mitochondria (Britten et al., 2000; Propper et al., 1999). Because in principle DLCs behave as expected in vivo, these results further emphasize the need for novel DLCs with higher therapeutic effectiveness. Our results showed that intraperitoneal injection of 20 mg/kg of F16 retarded the growth of A6-derived subcutaneous tumors in nude mice (V.R.F. and P.L., unpublished data). Thus, F16 might hold therapeutic potential as anticancer reagent.

Our screen has not only identified a novel small molecule with selective activity toward transformed cells, but it has identified the mitochondria as a compartment that is affected by *neu* overexpression. Using a panel of characterized mouse tumor cells, we could correlate increased $\Delta\psi_m$ to the specific transforming oncogene. *neu*-, v-Ha-*ras*-, and β-*catenin*-initiated tumors cells and *neu*-overexpressing EpH4 cells presented higher $\Delta\psi_m$ than c-*myc*-initiated tumor cell lines and nontransformed mammary epithelial cell lines. We have focused our efforts mainly on four oncogenes, and from that point of view, these are just examples of genetic alterations leading to changes in $\Delta\psi_m$. Prior to our analysis, chemically induced cellular transformation and overexpression of v-*fos* in rat fibroblasts are the only examples of a causal relationship between the initial transforming event and the increase in $\Delta\psi_m$ (Liang et al., 1999; Summerhayes et al., 1982; Zarbl et al., 1987).

To date, there is no clear understanding of what the key factors that contribute to differences in the magnitude of $\Delta\psi_m$ between tumor cells and their normal counterparts are. In a few cases, a link between oncogene expression and changes in the expression level of mitochondrial genes has been established (Ohnami et al., 1999). Thus, the variation of $\Delta\psi_m$ could simply come from differences in proteins involved in the respiratory chain or those that form the mitochondrial PTP (Modica-Napolitano and Aprille, 2001). On the other hand, differences in $\Delta\psi_m$ could be the consequence of metabolic adaptations that cells undergo during the process of cellular transformation (Dang and Semenza, 1999). It has been known since the 1930s that tumor cells maintain higher rates of anaerobic glycolysis even in the presence of high pO_2 levels (the so-called Warburg effect) (Warburg, 1956). Mitochondria generate ATP using the proton electrochemical gradient across their inner membrane. In theory, the inability of tumor cells to use mitochondria to fulfill all their ATP demands (i.e., dissipation of a smaller fraction $\Delta\mu H^+$) even when oxidative phosphorylation is not limited by the low pO_2 could explain why tumor cells display higher $\Delta\psi_m$. A systematic biochemical characterization of the mitochondrial protein profile of normal and transformed cells will provide us with clues to understand the basis for the altered $\Delta\psi_m$ in tumor cells and the correlation to oncogene overexpression. Knowing what proteins to inactivate in mitochondria of tumor cells, a target-limited search for compounds in a small molecule database could lead to more effective DLCs or to molecules that could be chemically modified to include the desired properties. In addition, if it were possible to transiently modulate the $\Delta\psi_m$, drug targeting could be improved and undesired side effects minimized.

Our analysis also suggests that in *neu*-overexpressing cells,

F16 was capable of neutralizing Neu activity and downstream signaling. It is quite possible that this effect is secondary to the mitochondrial damage imposed by the small molecule, since no direct interaction between F16 and Neu was detectable in Neu pull-down experiments (data not shown). Nevertheless, the growth promoting activity of the receptor could be blocked by F16 without specifically targeting the protein.

Finally, the fact that F16 specifically targets the mitochondria is of particular interest. Recently, attention has been drawn to mitochondria as potential targets of anticancer therapy, in particular because of their pivotal involvement in cell death (Costantini et al., 2000). As the molecular dissection of the apoptotic pathway proceeds, the crucial role of mitochondria in propagating the cell death signal becomes clearer (Green and Reed, 1998). Inactivation of the tumor suppressor *p53* and overexpression of the oncogene *bcl-2* are common traits in several neoplasias, conferring resistance to several apoptotic stimuli (Cheng et al., 2001; Korsmeyer et al., 1990; Somasundaram, 2000). Thus, therapeutic interventions that can selectively target the mitochondria of transformed cells and trigger the apoptotic cascade without relying on intact upstream apoptosis-inducing pathways could represent a specific, low toxicity approach in cancer treatment.

Experimental procedures

Reagents

Anti-phospho Neu, anti-Neu, and anti-pTyr were purchased from Upstate Biotechnology Inc. Anti-phospho MAP kinase, anti-PKB, and anti-phospho PKB were purchased from New England Biolabs. Anti-ERK-1 was obtained from Santa Cruz. F16 was obtained from Interbioscreen and Asinex, and the stocks combined and used where indicated in subsequent experiments.

Cell culture and generation of stable cell lines

EpH4 cells were grown in Dulbecco's modified Eagle's medium (DMEM), 10% FBS at 37°C/5% CO_2. EpH4 cells stably expressing *neu* were established. The *neu* transforming oncogene (*neu*^{T}) cDNA was subcloned into pRETRO-OFF (Clontech) as follows. A SalI/XhoI/HindIII/NotI adaptor was introduced into pBluescript (Stratagene). The HindIII/SalI fragment containing full-length *neu*^{T} cDNA was excised from a vector which itself was derived from pSV2neuNT and inserted into corresponding sites in p-Bluescript (Bargmann et al., 1986). Finally, the chimeric vector carrying *neu*^{T} cDNA was subjected to restriction digestion with NotI, and the excised 5 kb fragment including the *neu*^{T} cDNA was introduced into the NotI site in pRETRO-OFF. Transfection of EpH-4 cells was done using Fugene Reagent according to manufacturer's protocol (Boehinger Mannheim). Finally, stable clones were isolated by selection in medium containing puromycin (1.2 μg/ml). All the clones isolated showed constitutive level of Neu protein. No significant repression of Neu expression was observed upon doxycycline treatment.

Effect of F16 on cell proliferation

neu-initiated mouse tumors cell lines NF980, NF324-2A, NF324-1B, SMF, NAF, n-Neu, and Neu4145, v-Ha-*ras*-initiated tumor cell lines SH1.1, AC236, AC711, AC816, ACp53$^-$#1, ACp53$^-$#4782, AC222, AC99, AC260, ACp53$^-$#19, ACp53$^-$#16, AC/Balb6.6, AC/Balb14, and AC/Balb12, β-*catenin*-initiated tumor cell lines 5297.B2, 5281.1, 9281.a, and 5297.B1, and c-*myc*-initiated tumor cell lines 16MB9a, 13MA1a, Myc 83, and M158 were used to test the antiproliferative effect of F16. All these cell lines have been established in our laboratory from tumors dissected from v-Ha-*ras*-, *neu*-, c-*myc*-, and β-*catenin*-transgenic mice.

Human breast cancer cell lines MDA-MB231, MDA-MB435, MDA-MB436, MDA-MB453, MDA-MB-468, SKBR-3, MCF-7, T47D, and ZR-75-1 and mouse mammary epithelial cell line NMuMG obtained from the ATCC were used to test the antiproliferative effect of F16.

For quantitation purposes, for each cell line, 1×10^5 cells were seeded in each well of a 6-well plate. On the following day, 3 μM F16 was added to the medium, while control cells were left untreated. Cells were counted 3 days and 7 days after initiation of treatment. Counts were done in triplicate for untreated and F16-treated cells.

Cell lysate preparation and immunoblotting

EpH4, EpH4-A6, and EpH4-A8 were incubated in serum-free medium for 5 hr where indicated. Otherwise, cells were washed with PBS and lysed in lysis buffer (40 mM HEPES, 150 mM NaCl, 10 mM sodium pyrophosphate, 2% Nonidet P-40, 10 mM NaF, 2 mM EDTA, and 5 μM Na_3VO_4) containing Complete™ protease inhibitor cocktail (Roche). The lysates were spun at 140,000 × g for 30 min. to separate the insoluble material. Protein concentration was determined on the supernatants using Bradford reagent (Bio-Rad). An aliquot of each lysate containing equivalent amounts of protein was separated by SDS-PAGE and transferred to Immobilon-P membranes (Millipore). The transfer buffer consisted of 25 mM Tris, 190 mM glycine, 20% methanol, and 0.005% SDS. Membranes were blocked with 1.5% BSA in TBST (150 mM NaCl, 20 mM Tris-HCl [pH 7.4], and 0.3% Tween 20), and the primary antibodies (1 μg/ml) and secondary antibodies were in 0.2% BSA in the same buffer. Membranes were washed with TBST buffer. In all cases, blots were developed with horseradish peroxidase conjugated to anti-rabbit IgG or to anti-mouse IgG (Amersham). The enhanced chemiluminescence reagent (Pierce) was used for detection.

Cytoblot

A modified version of a protocol previously described was used for the cytoblot assay (Stockwell et al., 1999). Briefly, for this cytoblot assay, 2,000 control (EpH4-EV) and Neu overexpressing (EpH4-A6) cells in 40 μl of growing medium were seeded in duplicate in each well of a white 384-well plate (Costar). 16,000 compounds from a chemical library (ChemBridge) were transferred to each well to a final concentration of 10–15 μM. Plates were incubated at 37°C with 5% CO_2 for 36–40 hr. BrdU was then added to a final concentration of 20 μM and the cells were incubated at 37°C with 5% CO_2 for an additional 3 hr. Cells were then washed with PBS and fixed with 75% ethanol/25% TBS at 4°C for 1 hr. DNA denaturation was achieved by incubation with 2 M HCl/0.5% Tween-20 for 20 min, followed by neutralization with 2 M NaOH in Hank's Balanced Salt Solution (HBSS). Cells were subsequently washed with HBSS, blocked with PBS/0.3% Tween-20/1%BSA (PBSTB), and incubated with 0.5 μg/ml of mouse anti-BrdU antibody (PharMingen) and 1:5,000 dilution of anti-mouse IgG coupled to HRP in PBSTB for 1 hr at room temperature. Finally, the cells were washed with PBS, and 20 μl of 1:1 mix of the enhanced chemiluminescence reagent (Pierce) was then added to each well of a plate. Addition of reagents was done using a multidrop 384 liquid dispenser (Labsystems), and the washes were done using a plate washer (Bio-Tek Instruments). Chemiluminescent signal from each plate was detected by autoradiograph and multilabel counter Victor^2 (Wallac) in order to quantitate results.

Cell cycle analysis by flow cytometry

EpH4-EV, EpH4-A6, and various mouse tumor cell lines were incubated with 3 μM F16 for approximately 36 hr. In the case of human breast cancer cell lines, incubation with F16 was extended for a day, to a total of 3 days. Cells were next pulsed with BrdU (20 μM) for 1 hr and then fixed in 70% ethanol at −20°C overnight. The next morning, DNA was denatured in 2N HCl/0.5% TritonX-100. This procedure was followed by 2× washes 0.1 M $Na_2B_2O_7$, and 1× wash with PBS. Cells were resuspended in residual PBS, incubated with 20 μl of anti-BrdU/FITC (Becton Dickinson) for 1 hr, and subsequently washed 1× with PBS and resuspended in residual PBS. RNA was digested with RNaseA (1 μl of 10 mg/ml stock) at 37°C for 30 min. Finally, cells were diluted with 1 ml of 5 μg/ml propidium iodide/PBS and incubated for on ice for 15 min. The labeled cells were analyzed using the FACSCalibur (Becton-Dickinson).

Detection of apoptosis by Annexin V staining

EpH4-A6 and EpH4-EV cells untreated or treated with 3 μM F16 for 24, 48, and 72 hr were stained for 15 min with AnnexinV-PE conjugate in conjunction with the vital dye 7-amino-actinomycin D (7-AAD) following manufacturer's procedure (PharMingen). The labeled cells were analyzed using the FACSCalibur (Becton-Dickinson).

DNA fragmentation

DNA was isolated from 1×10^6 of untreated or F16 treated for 48, 60, and 72 hr using Suicide-Track™ (Oncogene) according to manufacturer's procedure. Samples were resolved by agarose gel electrophoresis and ethidium-bromide stained.

Cytochrome *c* release by immunofluorescence

Untreated or F16-treated A6 cells were washed and fixed with ice-cold 3.7% paraformaldehyde at RT, permeabilized with ice-cold 0.01% (v/v) Nonidet P-40 for 20 min, and incubated with 0.5% BSA/PBS for 15 min. Immunodetection was performed with monoclonal anti-cytochrome *c* antibody (PharMingen) and TRITC-conjugated anti-mouse secondary antibody (Jackson ImmunoResearch) in PBSTB. Cells were photographed under Axioskop microscope using a Spot Camera (Diagnostic Instruments). For the analysis of the effect of CsA on F16-induced cytochrome *c* release, A6 cells were incubated in the presence of 10 μM F16 and 10 μM CsA replenished into the medium every 30 min.

Localization of F16 in living cells

Cells grown on 60 mm plates were incubated with medium alone or medium containing 3 μM F16 for 24 hr at 37°C. The fluorescent signal of F16 was visualized under an Axiovert inverted microscope (Zeiss) using a standard fluorescein filter set and cells were photographed using a digital camera (Nikon D1).

Alternatively, for colocalization experiments, cells were treated as follows. 2×10^4 EpH4-EV and EpH4-A6 cells were seeded in 4-well chamber slides. The next morning, cells were left untreated or were treated with F16 at 3 μM for 2 hr. A mitochondrial specific stain, Mitotracker Red (Molecular Probes), was added to the medium to stain mitochondria, or Lysotracker Red (Molecular Probes) to stain lysosomes and acidic compartments according to manufacturer's procedure. Hoechst stain was also included in the medium to stain nuclei. Cells were photographed as previously described using an (100×) immersion oil objective (Zeiss). The effect of the protonophore FCCP (Sigma) on F16 accumulation was performed as previously done for colocalization experiments. EpH4-A6 cells preincubated with F16 (3 μM) were subsequently treated with 5 μM FCCP. Images were acquired immediately before and 1 min and 5 min after FCCP addition.

Determination of mitochondrial potential and mitochondrial mass

The mitochondrial membrane potential of various mouse cell lines was compared by flow cytometry, using the potentiometric probe tetramethylrhodamine methyl ester (TMRM, Molecular Probes) (Scaduto and Grotyohann, 1999). In all cases, cells were harvested and resuspended at 1×10^6 cells/ml in cell culture medium containing 10 μM verapamil and 100 μM probenecid (SIGMA) and MDR-1 and MRP-1 inhibitors respectively. TMRM was added to each tube to a final concentration of 50 nM. Cells were incubated at 37°C for 20 min and immediately analyzed by flow cytometry. In addition, cells were stained with nonyl-acridine orange (NAO) in order to estimate the mitochondrial mass in the cell lines probed with TMRM (Hiura et al., 2000). 1×10^6 cells/ml cells were incubated with 2 μM NAO for 20 min at 37°C. The fluorescent emission of NAO at 530 nm and 630 nm was collected. The ratio of green to red fluorescence best reflects the cardiolipin content of mitochondria.

Imaging of mitochondrial membrane potential

For imaging of mitochondrial membrane potential in situ, A6 and control cells were seeded onto 25 mm round glass coverslips at a density of 10^4 cells/coverslip and grown for 2 days prior to measurement. Cells were then stained with 20 nM TMRM dissolved in Hank's balanced salt solution (HBSS) with 10% FCS, 10 mM HEPES, and 5 μM verapamil (Sigma) for 20 min at 37°C. Coverslips were placed on the stage of a Nikon Eclipse TE300 inverted microscope equipped with a Xenon-lamp illumination system and with a Hamamatsu Orca ER 12-bit digital cooled CCD camera. Cells were excited at 530 ± 2.5 using a Polychome IV monochromator (Till Photonics), and emitted light was collected using a 560 longpass filter. Digital images were acquired with exposure times of 30 msec using a 60×, 1.4 NA Plan Apo oil immersion objective (Nikon). Data analysis was done using Metamorph software (Universal Imaging).

Electron microscopy

Cells grown in 35 mm dishes were left untreated or treated with 3 μM F16 for the indicated times, and fixed for 1 hr at room temperature in 0.1 M Cacodylate buffer containing 1.25% formaldehyde, 2.5% glutaraldehyde, and 0.3% picric acid. Samples were then treated with 1% osmiuntetroxide/1.5% potassiumferrocyanide followed by 1% uranyl acetate, dehydrated, and epon-araldite embedded. Ultrathin sections were examined using a JEOL 1200EX microscope. For the analysis of the effect of CsA on F16-induced swelling, A6 cells were incubated in the presence of 10 μM F16 and 10 μM CsA replenished into the medium every 30 min.

Determination of ATP

Cellular ATP levels were determined by luciferin-luciferase method using the ATP Bioluminescence Assay Kit (Roche). EpH4-EV and EpH4-A6 cells were grown in the absence or in the presence of 3 μM F16 for 15 and 24 hr. As a control, A6 were treated with 5 μM FCCP (Sigma) for 24 hr. Cells were then harvested and equivalent numbers of cells were used for each determination, according to manufacturer's procedure. Each determination was done in triplicate, and the entire experiment was performed twice.

Measurement of intracellular superoxide anion

Changes in the levels of intracellular oxidants were investigated using the fluorescent probe dihydroethidium (DHE) (Molecular Probes). Superoxide anions can oxidize DHE to ethidium bromide (EtBr), which binds to DNA. An increase in the fluorescence of EtBr/DNA is suggestive of superoxide generation (Vanden Hoek et al., 1998). EpH4-EV and EpH4-A6 cells were grown in the absence or in the presence of 3 μM F16 for 15, 24, 48, and 72 hr cells were resuspended and diluted to 10^6 cells/ml. DHE was added to the cell suspension to a final 2 μM in each case. Cells were incubated at 37°C for 15 min and immediately analyzed by flow cytometry using the Epics Altra (Beckman-Coulter).

Isolation of mitochondria, mitochondrial swelling membrane potential, and respiration determination

Mitochondria were isolated from livers of Balb/c7 mice by standard differential centrifugation, and resuspended in isolation buffer (0.2 M sucrose, 10 mM Tris-MOPS [pH 7.4], 0.1 mM EGTA-Tris, and 0.1% delipidated BSA) (Costantini et al., 1995). For swelling determination, changes in side scatter at 545 ± 2.5 nm of a 0.5 mg/ml suspension of mitochondria in experimental buffer (125 mM KCl, 10 mM Tris-MOPS [pH 7.4], 1 mM Pi, 5 mM glutamate, 2.5 mM malate, and 10 μM EGTA-Tris [pH 7.4]) were monitored by using a LS-50B spectrofluorimeter. To monitor changes in mitochondrial membrane potential, we took advantage of the intrinsic potentiometric properties of F16. Mitochondria (0.5 mg/ml) were incubated in experimental buffer with the indicated concentrations of F16, and changes in F16 fluorescence intensity were measured using a LS-50B spectrofluorimeter at 25°C, with excitation and emission wavelengths set at 415 ± 2.5 nm and 520 ± 5 nm, respectively. All measurements were performed at 25°C, and the instrument was equipped with magnetic stirring.

Oxygen consumption was determined using a Clarke-type oxygen electrode equipped with thermostatic control and magnetic stirring. Mitochondria (1 mg/ml) were incubated in experimental buffer supplemented with substrates for each respiratory chain complex as indicated in Figure 6: 5 mM glutamate plus 2.5 mM malate for complex I, 5 mM succinate-Tris in the presence of 2 μM rotenone for complex II+III, 3 mM ascorbate plus 150 μM TMPD in the presence of 1 μg/ml antimycin A for complex IV.

Acknowledgments

We thank Juanita Campos and Maria Ericsson for expert assistance in flow cytometry and electron microscopy, respectively. Montserrat Michelman has provided helpful assistance in determining F16 sensitivity on cultured cell lines. Dr. Aya Leder and Dr. Jennifer Michaelson have kindly provided several of the tumor cell lines tested. We are also grateful to Dr. Randall King for his advice during the HTS and to Dr. Nicholas Chester and Dr. Robert Weiss for helpful discussions on this manuscript. L.S. is a Human Frontier Science Program Long Term Fellow.

Received: April 9, 2002
Revised: May 21, 2002

References

Anderson, W.M., Patheja, H.S., Delinck, D.L., Baldwin, W.W., Smiley, S.T., and Chen, L.B. (1989). Inhibition of bovine heart mitochondrial and Paracoccus denitrificans NADH-ubiquinone reductase by dequalinium chloride and three structurally related quinolinium compounds. Biochem. Int. *19*, 673–685.

Anderson, W.M., Delinck, D.L., Benninger, L., Wood, J.M., Smiley, S.T., and Chen, L.B. (1993). Cytotoxic effect of thiacarbocyanine dyes on human colon carcinoma cells and inhibition of bovine heart mitochondrial NADH-ubiquinone reductase activity via a rotenone-type mechanism by two of the dyes. Biochem. Pharmacol. *45*, 691–696.

Bachelder, R.E., Wendt, M.A., Fujita, N., Tsuruo, T., and Mercurio, A.M. (2001). The cleavage of Akt/protein kinase B by death receptor signaling is an important event in detachment-induced apoptosis. J. Biol. Chem. *276*, 34702–34707.

Bargmann, C.I., Hung, M.C., and Weinberg, R.A. (1986). The neu oncogene encodes an epidermal growth factor receptor-related protein. Nature *319*, 226–230.

Baselga, J. (2001). Phase I and II clinical trials of trastuzumab. Ann. Oncol. *12*, S49–S55.

Bernal, S.D., Lampidis, T.J., Summerhayes, I.C., and Chen, L.B. (1982). Rhodamine-123 selectively reduces clonal growth of carcinoma cells in vitro. Science *218*, 1117–1119.

Bernardi, P., Scorrano, L., Colonna, R., Petronilli, V., and Di Lisa, F. (1999). Mitochondria and cell death. Mechanistic aspects and methodological issues. Eur. J. Biochem. *264*, 687–701.

Boitier, E., Rea, R., and Duchen, M.R. (1999). Mitochondria exert a negative feedback on the propagation of intracellular Ca2+ waves in rat cortical astrocytes. J. Cell Biol. *145*, 795–808.

Britten, C.D., Rowinsky, E.K., Baker, S.D., Weiss, G.R., Smith, L., Stephenson, J., Rothenberg, M., Smetzer, L., Cramer, J., Collins, W., et al. (2000). A phase I and pharmacokinetic study of the mitochondrial-specific rhodacyanine dye analog MKT 077. Clin. Cancer Res. *6*, 42–49.

Broekemeier, K.M., Dempsey, M.E., and Pfeiffer, D.R. (1989). Cyclosporin A is a potent inhibitor of the inner membrane permeability transition in liver mitochondria. J. Biol. Chem. *264*, 7826–7830.

Cheng, E.H., Wei, M.C., Weiler, S., Flavell, R.A., Mak, T.W., Lindsten, T., and Korsmeyer, S.J. (2001). BCL-2, BCL-X(L) sequester BH3 domain-only molecules preventing BAX- and BAK-mediated mitochondrial apoptosis. Mol. Cell *8*, 705–711.

Chiba, Y., Kubota, T., Watanabe, M., Matsuzaki, S.W., Otani, Y., Teramoto, T., Matsumoto, Y., Koya, K., and Kitajima, M. (1998). MKT-077, localized lipophilic cation: antitumor activity against human tumor xenografts serially transplanted into nude mice. Anticancer Res. *18*, 1047–1052.

Costantini, P., Petronilli, V., Colonna, R., and Bernardi, P. (1995). On the effects of paraquat on isolated mitochondria. Evidence that paraquat causes opening of the cyclosporin A-sensitive permeability transition pore synergistically with nitric oxide. Toxicology *99*, 77–88.

Costantini, P., Jacotot, E., Decaudin, D., and Kroemer, G. (2000). Mitochondrion as a novel target of anticancer chemotherapy. J. Natl. Cancer Inst. *92*, 1042–1053.

Dang, C.V., and Semenza, G.L. (1999). Oncogenic alterations of metabolism. Trends Biochem. Sci. *24*, 68–72.

Green, D.R., and Reed, J.C. (1998). Mitochondria and apoptosis. Science *281*, 1309–1312.

Gross, A., McDonnell, J.M., and Korsmeyer, S.J. (1999). BCL-2 family members and the mitochondria in apoptosis. Genes Dev. *13*, 1899–1911.

Hiura, T.S., Li, N., Kaplan, R., Horwitz, M., Seagrave, J.C., and Nel, A.E. (2000). The role of a mitochondrial pathway in the induction of apoptosis by chemicals extracted from diesel exhaust particles. J. Immunol. *165*, 2703–2711.

Hynes, N.E., and Stern, D.F. (1994). The biology of erbB-2/neu/HER-2 and its role in cancer. Biochim. Biophys. Acta *1198*, 165–184.

Korsmeyer, S.J., McDonnell, T.J., Nunez, G., Hockenbery, D., and Young, R. (1990). Bcl-2: B cell life, death and neoplasia. Curr. Top. Microbiol. Immunol. *166*, 203–207.

Koya, K., Li, Y., Wang, H., Ukai, T., Tatsuta, N., Kawakami, M., Shishido, T., and Chen, L.B. (1996). MKT-077, a novel rhodacyanine dye in clinical trials, exhibits anticarcinoma activity in preclinical studies based on selective mitochondrial accumulation. Cancer Res. *56*, 538–543.

Kroemer, G., Dallaporta, B., and Resche-Rigon, M. (1998). The mitochondrial death/life regulator in apoptosis and necrosis. Annu. Rev. Physiol. *60*, 619–642.

Lane, H.A., Beuvink, I., Motoyama, A.B., Daly, J.M., Neve, R.M., and Hynes, N.E. (2000). ErbB2 potentiates breast tumor proliferation through modulation of p27(Kip1)-Cdk2 complex formation: receptor overexpression does not determine growth dependency. Mol. Cell. Biol. *20*, 3210–3223.

Liang, B.C., Miller, L., and Weller, A. (1999). Ethyl-nitrosourea transformed astrocytes exhibit mitochondrial membrane hyperpolarization and constrained apoptosis. Apoptosis *4*, 89–97.

Liu, X., Kim, C.N., Yang, J., Jemmerson, R., and Wang, X. (1996). Induction of apoptotic program in cell-free extracts: requirement for dATP and cytochrome c. Cell *86*, 147–157.

Lizard, G., Chignol, M.C., Chardonnet, Y., and Schmitt, D. (1994). Active cell membrane mechanisms involved in the exclusion of Rh 123 allow distinction between normal and tumoral cells. Cell Biol. Toxicol. *10*, 399–406.

Moasser, M.M., Basso, A., Averbuch, S.D., and Rosen, N. (2001). The tyrosine kinase inhibitor ZD1839 ("Iressa") inhibits HER2-driven signaling and suppresses the growth of HER2-overexpressing tumor cells. Cancer Res. *61*, 7184–7188.

Modica-Napolitano, J.S., and Aprille, J.R. (1987). Basis for the selective cytotoxicity of rhodamine 123. Cancer Res. *47*, 4361–4365.

Modica-Napolitano, J.S., and Aprille, J.R. (2001). Delocalized lipophilic cations selectively target the mitochondria of carcinoma cells. Adv. Drug Deliv. Rev. *49*, 63–70.

Modica-Napolitano, J.S., Weiss, M.J., Chen, L.B., and Aprille, J.R. (1984). Rhodamine 123 inhibits bioenergetic function in isolated rat liver mitochondria. Biochem. Biophys. Res. Commun. *118*, 717–723.

Modica-Napolitano, J.S., Koya, K., Weisberg, E., Brunelli, B.T., Li, Y., and Chen, L.B. (1996). Selective damage to carcinoma mitochondria by the rhodacyanine MKT-077. Cancer Res. *56*, 544–550.

Muller, W.J., Sinn, E., Pattengale, P.K., Wallace, R., and Leder, P. (1988). Single-step induction of mammary adenocarcinoma in transgenic mice bearing the activated c-neu oncogene. Cell *54*, 105–115.

Nadakavukaren, K.K., Nadakavukaren, J.J., and Chen, L.B. (1985). Increased rhodamine 123 uptake by carcinoma cells. Cancer Res. *45*, 6093–6099.

Neve, R.M., Lane, H.A., and Hynes, N.E. (2001). The role of overexpressed HER2 in transformation. Ann. Oncol. *12*, S9–S13.

Noonberg, S.B., and Benz, C.C. (2000). Tyrosine kinase inhibitors targeted to the epidermal growth factor receptor subfamily: role as anticancer agents. Drugs *59*, 753–767.

Ohnami, S., Matsumoto, N., Nakano, M., Aoki, K., Nagasaki, K., Sugimura, T., Terada, M., and Yoshida, T. (1999). Identification of genes showing differential expression in antisense K-ras-transduced pancreatic cancer cells with suppressed tumorigenicity. Cancer Res. *59*, 5565–5571.

Olayioye, M.A., Neve, R.M., Lane, H.A., and Hynes, N.E. (2000). The ErbB signaling network: receptor heterodimerization in development and cancer. EMBO J. *19*, 3159–3167.

Propper, D.J., Braybrooke, J.P., Taylor, D.J., Lodi, R., Styles, P., Cramer, J.A., Collins, W.C., Levitt, N.C., Talbot, D.C., Ganesan, T.S., and Harris, A.L.

(1999). Phase I trial of the selective mitochondrial toxin MKT077 in chemo-resistant solid tumours. Ann. Oncol. *10*, 923–927.

Raha, S., and Robinson, B.H. (2001). Mitochondria, oxygen free radicals, and apoptosis. Am. J. Med. Genet. *106*, 62–70.

Reichmann, E., Schwarz, H., Deiner, E.M., Leitner, I., Eilers, M., Berger, J., Busslinger, M., and Beug, H. (1992). Activation of an inducible c-FosER fusion protein causes loss of epithelial polarity and triggers epithelial-fibroblastoid cell conversion. Cell *71*, 1103–1116.

Roh, H., Pippin, J., and Drebin, J.A. (2000). Down-regulation of HER2/neu expression induces apoptosis in human cancer cells that overexpress HER2/neu. Cancer Res. *60*, 560–565.

Rubin, I., and Yarden, Y. (2001). The basic biology of HER2. Ann. Oncol. *12*, S3–S8.

Scaduto, R.C., Jr., and Grotyohann, L.W. (1999). Measurement of mitochondrial membrane potential using fluorescent rhodamine derivatives. Biophys. J. *76*, 469–477.

Scorrano, L., Petronilli, V., and Bernardi, P. (1997). On the voltage dependence of the mitochondrial permeability transition pore. A critical appraisal. J. Biol. Chem. *272*, 12295–12299.

Scorrano, L., Petronilli, V., Colonna, R., Di Lisa, F., and Bernardi, P. (1999). Chloromethyltetramethylrosamine (Mitotracker Orange) induces the mitochondrial permeability transition and inhibits respiratory complex I. Implications for the mechanism of cytochrome c release. J. Biol. Chem. *274*, 24657–24663.

Seymour, L.K. (2001). Epidermal growth factor receptor as a target: recent developments in the search for effective new anti-cancer agents. Curr. Drug Targets *2*, 117–133.

Somasundaram, K. (2000). Tumor suppressor p53: regulation and function. Front. Biosci. *5*, D424–D437.

Stockwell, B.R., Haggarty, S.J., and Schreiber, S.L. (1999). High-throughput screening of small molecules in miniaturized mammalian cell-based assays involving post-translational modifications. Chem. Biol. *6*, 71–83.

Summerhayes, I.C., Lampidis, T.J., Bernal, S.D., Nadakavukaren, J.J., Nadakavukaren, K.K., Shepherd, E.L., and Chen, L.B. (1982). Unusual retention of rhodamine 123 by mitochondria in muscle and carcinoma cells. Proc. Natl. Acad. Sci. USA *79*, 5292–5296.

Sun, X., Wong, J.R., Song, K., Hu, J., Garlid, K.D., and Chen, L.B. (1994). AA1, a newly synthesized monovalent lipophilic cation, expresses potent in vivo antitumor activity. Cancer Res. *54*, 1465–1471.

Tikhomirov, O., and Carpenter, G. (2001). Caspase-dependent cleavage of ErbB-2 by geldanamycin and staurosporin. J. Biol. Chem. *276*, 33675–33680.

Vanden Hoek, T.L., Becker, L.B., Shao, Z., Li, C., and Schumacker, P.T. (1998). Reactive oxygen species released from mitochondria during brief hypoxia induce preconditioning in cardiomyocytes. J. Biol. Chem. *273*, 18092–18098.

Warburg, O. (1956). On the origin of cancer cells. Science *123*, 309–314.

Wei, M.C., Zong, W.X., Cheng, E.H., Lindsten, T., Panoutsakopoulou, V., Ross, A.J., Roth, K.A., MacGregor, G.R., Thompson, C.B., and Korsmeyer, S.J. (2001). Proapoptotic BAX and BAK: a requisite gateway to mitochondrial dysfunction and death. Science *292*, 727–730.

Winer, E.P., and Burstein, H.J. (2001). New combinations with herceptin((r)) in metastatic breast cancer. Oncology *61* (*Suppl*.), 50–57.

Yarden, Y. (2001). Biology of HER2 and its importance in breast cancer. Oncology *61* (*Suppl*.), 1–13.

Zarbl, H., Latreille, J., and Jolicoeur, P. (1987). Revertants of v-fos-transformed fibroblasts have mutations in cellular genes essential for transformation by other oncogenes. Cell *51*, 357–369.

Zwick, E., Bange, J., and Ullrich, A. (2001). Receptor tyrosine kinase signalling as a target for cancer intervention strategies. Endocr. Relat. Cancer *8*, 161–173.